

## Evaluating the relationship between the area and latitude of large igneous provinces and Earth's long-term climate state

Yuem Park<sup>1</sup>, Nicholas L. Swanson-Hysell<sup>1</sup>, Lorraine E. Lisiecki<sup>2</sup>, Francis A. Macdonald<sup>2</sup>

<sup>1</sup> Department of Earth and Planetary Science, University of California, Berkeley, CA, USA

<sup>2</sup> Department of Earth Science, University of California, Santa Barbara, CA, USA

*This article is in review for the AGU book entitled Environmental Change and Large Igneous Provinces: The Deadly Kiss of LIPs.*

### <sup>1</sup> ABSTRACT

One of the hypothesized effects of large igneous provinces (LIPs) is planetary cooling on million-year timescales associated with enhanced silicate weathering of the freshly-emplaced basalt. This study combines reconstructions of the original surface extent and emplacement ages of LIPs, a paleogeographic model, and a parameterization of LIP erosion to estimate LIP area in all latitudinal bands through the Phanerozoic. This analysis reveals no significant correlation between total LIP area, nor LIP area in the tropics, and the extent of continental ice sheets. The largest peaks in tropical LIP area are at times of non-glacial climate. These results suggest that changes in planetary weatherability associated with LIPs are not the fundamental control on whether Earth is in a glacial or non-glacial climate, although they could provide a secondary modulating effect in conjunction with other processes.

## <sup>12</sup> INTRODUCTION

<sup>13</sup> Global weatherability is the sum of factors aside from climate itself that contribute to overall  
<sup>14</sup> global weathering and associated CO<sub>2</sub> consumption, such as the latitudinal distribution of  
<sup>15</sup> continents and mountain belts (Kump and Arthur, 1997). On a planet with high weatherability,  
<sup>16</sup> the CO<sub>2</sub> input from volcanism can be removed via silicate weathering at a lower atmospheric CO<sub>2</sub>  
<sup>17</sup> concentration than on a less weatherable planet. Basaltic regions consume more CO<sub>2</sub> than regions  
<sup>18</sup> where the bedrock composition is closer to bulk continental crust because mafic lithologies have  
<sup>19</sup> relatively high concentrations of Ca and Mg (that ultimately sequester carbon through  
<sup>20</sup> precipitation as carbonate), constitute minerals with relatively high reactivity (Gislason and  
<sup>21</sup> Oelkers, 2003), and have relatively high weathering rates (Dessert et al., 2003; Ibarra et al., 2016).  
<sup>22</sup> Furthermore, data from basaltic watersheds show that chemical weathering rates are highest in  
<sup>23</sup> regions with high runoff and temperature. As a result, CO<sub>2</sub> consumption in basaltic regions is  
<sup>24</sup> most pronounced in the tropical rain belt (Dessert et al., 2003; Hartmann et al., 2009, 2014).

<sup>25</sup> One aspect of large igneous province (LIP) emplacement that has been hypothesized to relate  
<sup>26</sup> to long-term global climate is the effect that associated mafic lithologies could have on increasing  
<sup>27</sup> global weatherability and driving cooling. In particular, the emplacement of LIPs in the tropics  
<sup>28</sup> has been hypothesized to be associated with specific episodes of climatic cooling on Earth. In the  
<sup>29</sup> Neoproterozoic, the emplacement of the ca. 720 Ma Franklin LIP in the tropics, in concert with  
<sup>30</sup> elevated runoff rates associated with supercontinent break-up, has been implicated as a major  
<sup>31</sup> contributor to the cooling that initiated the Sturtian ‘Snowball Earth’ (Donnadieu et al., 2004a;  
<sup>32</sup> Macdonald et al., 2010; Cox et al., 2016). In the Cenozoic, the movement of the Deccan LIP into  
<sup>33</sup> the tropical rain belt, together with the low-latitude emplacement of the Ethiopian Traps, has  
<sup>34</sup> been implicated in drawing down CO<sub>2</sub> levels in the lead-up to Oligocene glaciation of Antarctica  
<sup>35</sup> (Kent and Muttoni, 2008, 2013). More recently, Johansson et al. (2018) used paleogeographic  
<sup>36</sup> reconstructions to suggest that tropical LIP area correlates with Phanerozoic climate change  
<sup>37</sup> through comparison with a pCO<sub>2</sub> proxy compilation.

38 This chapter seeks to address two interconnected questions: 1) how unique are the peaks in  
39 low-latitude LIP area that have been proposed to be associated with climatic cooling?; and 2)  
40 how strong is the overall relationship between tropical LIP area and glaciation?

41 **METHODS**

42 This study combines reconstructions of the original surface extent and emplacement ages of LIPs,  
43 a paleogeographic model, and a parameterization of LIP erosion to estimate LIP area in all  
44 latitudinal bands through the Phanerozoic. We then compare these time series of zonal LIP area  
45 to the latitudinal extent of continental ice sheets - a proxy for Earth's long term climate state.  
46 This study builds upon a zonal LIP area analysis presented in the supplementary materials for  
47 Macdonald et al. (2019) by more rigorously developing parameterizations of LIP erosion and  
48 exploring several geologically reasonable LIP post-emplacement scenarios.

49 Outlines of the original surface extent of continental LIPs through the Phanerozoic (Fig. 1)  
50 were slightly modified (to ensure that all currently exposed volcanic lithologies are encapsulated  
51 by the initial LIP area polygons) from the compilation of Ernst and Youbi (2017) and Ernst  
52 (2019), and emplacement ages were taken from the literature (Table 1). The LIP original surface  
53 extent compilation seeks to reconstruct the original surface extent of LIPs with the caveat that  
54 there can be significant uncertainty with doing so, particularly for older more deeply eroded LIPs.  
55 These polygons encapsulate all of the preserved rocks associated with a given LIP, including  
56 dikes, sills, and layered intrusions, in addition to subaerial volcanics (Fig. 1). For some LIPs, this  
57 approach may lead to an over-estimate of original surface extent, given that subsurface intrusions  
58 could extend over a broader area than the surface volcanics. The polygons also assume complete  
59 surface coverage between wide-spread remnants, creating further potential for these original  
60 extent outlines to be over-estimates. These original extent outlines could also under-estimate the  
61 surface area for some LIPs where flows have been eroded and feeder dikes are not exposed or  
62 poorly documented. However, despite these uncertainties, this approach likely provides the best

63 estimates available of original surface extent for ancient LIPs. The extents of presently-exposed  
64 volcanics associated with LIPs that were used for present-day area estimates (Fig. 1) and the  
65 sources that went into the construction of the original extent polygons by Ernst and Youbi (2017)  
66 and Ernst (2019) were taken from a number of resources including the PLATES compilation  
67 (Coffin et al., 2006) and more recent compilation efforts associated with the LIPs Reconstruction  
68 Project (Ernst et al., 2013; Table 1).

69 After LIPs are emplaced, they progressively erode. In order to account for the associated  
70 decrease in area with time, Goddériss et al. (2017b) took the approach of fitting an exponential  
71 decay function to estimates of the original surface extent and the current surface extent of 5 LIPs.  
72 They used the resulting exponential decay constants to develop a first-order parameterization of  
73 changing LIP area through time. We extend this approach to 19 basaltic LIPs for which there are  
74 estimates of the original surface extent of the province and the current surface extent of rocks  
75 associated with the province (Fig. 2). While there are significant uncertainties associated with  
76 the area estimates, this compilation suggests that an exponential decay function is an appropriate  
77 first-order representation of the progressive reduction in LIP area (Fig. 2). The best-fit  
78 exponential function results in a LIP area half-life of 29 Myr. However, since we explicitly  
79 account for LIP burial separately in our area analysis (see below), we exclude from our estimation  
80 of a representative LIP area half-life the 6 of 19 LIPs which are inferred to have been partially or  
81 completely buried. This latter approach yields a slightly longer best-fit half-life of 36 Myr (Fig.  
82 2). Although the exponential fit to the 13 unburied LIPs is good (i.e. it yields a low root mean  
83 square error of 0.14), if each LIP is fit individually with an exponential decay function, there is  
84 variability in the estimated half-lives from ~20 Myr up to ~120 Myr for the Deccan Traps (Table  
85 1). In the analysis of LIP area through time, we implement decay scenarios informed by these  
86 results: the ' $t_{1/2} = 36$  Myr' scenario uses the best-fit half-life of 36 Myr, while the ' $t_{1/2} =$   
87 120 Myr' scenario uses the slower decay. Given that the post-emplacement weathering and  
88 erosional history of each LIP should be dependent on the tectonic and climatic setting that each  
89 LIP experiences during and after emplacement, this approach is simplistic, but it provides a

90 framework for analysis. The LIP reconstructions used in this study also include pre-Phanerozoic  
91 LIPs. However, given the imposed exponential decay since emplacement, the inclusion of these  
92 LIPs does not significantly influence the calculated LIP areas through the Phanerozoic, which is  
93 the focus of this analysis.

94 Of the tectonic factors that could alter exposed LIP area, the most consequential is  
95 near-immediate burial by sediment of LIP volcanics that are co-located with a rift basin. There  
96 are numerous examples in the record where there is partial or complete burial of a LIP associated  
97 with rifting and thermal subsidence (Table 1). For example, the Afar LIP is both associated with  
98 the Ethiopian Traps which form plateau flood basalts as well as successful rifting in the region of  
99 the Red Sea that has resulted in burial (Fig. 1). To account for the rapid decrease in exposed  
100 surface area that would result from burial by sediments in a rift basin, we impose two different  
101 burial scenarios for LIPs that are co-located with rifting. The ‘50% burial’ scenario imposes  
102 instantaneous burial of 50% of the LIP area while the ‘100% burial’ imposes instantaneous burial  
103 of the entire LIP as an end-member scenario. A limitation of our treatment of LIPs that are  
104 co-located with rifting is that we ‘bury’ all of these LIPs instantly at the time of emplacement  
105 and to the same degree when in fact the degree and timing of burial of these LIPs may vary  
106 substantially. The LIP area analysis uses all of the available combinations of the distinct decay  
107 and burial scenarios described above.

108 Our LIP reconstruction differs from that of Johansson et al. (2018). In contrast to the decay  
109 and decay+burial scenarios implemented on estimates of original LIP extent in this study,  
110 Johansson et al. (2018) uses a static extent for each LIP throughout the reconstruction. In their  
111 analysis, some of the polygons correspond to the present-day surface extent and some represent  
112 the original extent that includes currently buried portions of the LIP (e.g. the Keweenawan  
113 Midcontinent Rift for which the implemented extent in Johansson et al., 2018 is from geophysical  
114 data that largely corresponds to buried subsurface exposures).

115 The original surface extent LIP polygons were assigned a plate ID corresponding to a tectonic

116 unit on Earth using the polygons of Torsvik and Cocks (2016) for the Phanerozoic. The LIP  
117 polygons and tectonic units were reconstructed from 520 Ma to the present (e.g. Fig. 5) utilizing  
118 the paleogeographic model of Torsvik and Cocks (2016) in the spin axis reference frame (anchor  
119 plate ID of 1). This paleogeographic model was updated to include revisions to Ordovician  
120 Laurentia (Swanson-Hysell and Macdonald, 2017) and Paleozoic Asia (Domeier, 2018).  
121 Reconstructions and area calculations within latitude bands utilized the pyGPlates function  
122 library and custom Python scripts. The total LIP area and the LIP area reconstructed within the  
123 tropical rain belt were calculated for the various decay and burial scenarios at a resolution of  
124 5 Myr (Fig. 4B and C). All the data and code necessary to reproduce the analyses and figures  
125 presented in this study can be downloaded from GitHub  
126 ([https://github.com/Swanson-Hysell-Group/Large\\_Igneous\\_Provinces](https://github.com/Swanson-Hysell-Group/Large_Igneous_Provinces)) and are also archived in  
127 the Zenodo repository (URL TO BE ADDED HERE).

128 The ascent of air near the equator associated with Earth's large-scale Hadley circulation  
129 promotes precipitation and leads to a low-latitude band of high rainfall known as the tropical rain  
130 belt. In contrast, the descending branches of the Hadley circulation in the subtropics are  
131 associated with aridity (Manabe, 1969). We use 15° S to 15° N as a working definition of the  
132 tropical rain belt, as these latitudes approximately correspond with a sharp increase in zonal  
133 mean precipitation when approaching the equator to values greater than 1.0 m/yr in modern  
134 climatological data (Kalnay et al., 1996; Fig. 3). Other parameters that could be used to define  
135 the tropical rain belt are runoff and precipitation minus evaporation (P-E). When approaching  
136 the equator in modern climatological data, zonal mean runoff sharply increases to values above  
137 0.25 m/yr between approximately ±10° and ±15° (Fekete et al., 1999; Fig. 3), and zonal mean  
138 P-E sharply increases to values above 0.5 m/yr also between approximately ±10° and ±15°  
139 (Trenberth et al., 2011; Fig. 3). While seasonally high precipitation within ±15° of the equator  
140 associated with migration of the intertropical convergence zone could be a driver of high chemical  
141 weathering, annual mean runoff is often the value that is used within parameterizations of  
142 chemical weathering (e.g. West, 2012). Using runoff or P-E favors a definition of the tropical rain

143 belt that is closer to  $\pm 10^\circ$  rather than  $\pm 15^\circ$ . Therefore, we tested the sensitivity of our results to  
144 the assumed width of the tropical rain belt by performing the tropical LIP area calculations with  
145 a tropical rain belt width of  $\pm 10^\circ$ . We also calculated the area of LIPs within  $\pm 20^\circ$  of the equator  
146 (a width that includes part of the arid subtropics) in order to account for uncertainties in the  
147 paleolatitude of LIPs in the paleogeographic model. We find that both of these additional  
148 analyses (LIP area calculated within  $\pm 10^\circ$  and  $\pm 20^\circ$  of the equator) yield similar results to those  
149 obtained when LIP area is calculated within  $\pm 15^\circ$  of the equator (Table 2).

150 In Evans (2006), the reconstructed paleolatitudes of basins with thick, basin-wide evaporite  
151 deposition are shown to be consistently in the subtropics throughout the Phanerozoic and the  
152 Proterozoic, suggesting that the large-scale atmospheric circulation that gives rise to intense  
153 precipitation in the tropical rain belt and an arid subtropical climate is stable through time.  
154 However, subsequent work by Boucot et al. (2013) and Cao et al. (2018) has interpreted evaporite  
155 deposits to have formed at or near the equator at times in the Phanerozoic. While some of this  
156 variability could be attributed to waxing/waning of the width of the tropical rain belt as a whole,  
157 it is important to note that there can be large deviations in local precipitation from the zonal  
158 mean due to factors such as monsoon-related precipitation (Trenberth et al., 2000), or  
159 continentality (i.e. how dispersed or amalgamated the continents are) which can lead to aridity in  
160 continental interiors. For instance, much of the Early Cretaceous low-latitude evaporite deposits  
161 were formed in basins that were located deep within arid continental interiors at the time of  
162 deposition (Boucot et al., 2013; Cao et al., 2018). Furthermore, in contrast to Evans (2006), the  
163 compilation of evaporite deposits of Boucot et al. (2013) contains sedimentary sequences in which  
164 the occurrence of evaporitic minerals is limited (e.g. to disseminated gypsum pseudomorphs).  
165 Such limited evaporitic mineral precipitation could be attributed to seasonal evaporation that  
166 transiently led to saturation states that otherwise would not be expected for that latitude.  
167 Nevertheless, a limitation of the LIP analysis described in this study is that it does not account  
168 for deviations in local precipitation from the zonal mean (due to the infeasibility of running a  
169 highly-resolved global climate model at each time-step in the analysis). However, evaporite

170 deposits, including those in which the occurrence of evaporitic minerals is limited, are distributed  
171 bimodally about the equator in the subtropics for the vast majority of the past ~420 Myr (Cao  
172 et al., 2018) and overall stability of the large-scale atmospheric circulation is predicted by climate  
173 dynamics (Donohoe and Voigt, 2017). Therefore, the assumption of enhanced precipitation and  
174 runoff in the tropics throughout the Phanerozoic is warranted.

175 To evaluate the relationship between Earth's climate state and total and tropical LIP area, we  
176 compared these areas to a compilation of the latitudinal extent of continental ice sheets over the  
177 Phanerozoic (Macdonald et al., 2019; Fig. 4E). The goal in doing so is to evaluate the hypothesis  
178 that there is a correlation between LIP area in the tropics and Earth's long-term climate state.  
179 The land ice record is an imperfect tracker of climate as it is insensitive to changes in temperature  
180 during non-glacial intervals, is influenced by additional factors such as the physical geography of  
181 the continents during glacial intervals, and is potentially vulnerable to removal from the  
182 observable geologic record via erosion and burial. Furthermore, the threshold  $p\text{CO}_2$  for  
183 establishing a glacial climate is dependent on ocean circulation and changing solar luminosity (e.g.  
184 Shevenell, 2004; DeConto et al., 2008). Nevertheless, it forms a physical record of Earth's climate  
185 through time and delineates glacial and non-glacial climate states. We take two approaches for  
186 comparison between the LIP area reconstructions and the record of ice extent. The first is to  
187 calculate the Pearson correlation coefficient between LIP area and the extent of ice away from the  
188 pole. The second is to consider the degree of overlap between intervals of high LIP area (defined  
189 as LIP area >30% of the maximum in a given post-emplacement model) and intervals of glacial  
190 climate (defined as ice extent >10° from the poles). This overlap approach places less emphasis on  
191 the specific magnitudes of the peaks in the compiled ice extent and LIP area records.

192 Another approach would be to compare the LIP area reconstructions to proxy compilations of  
193  $p\text{CO}_2$  (as done by Johansson et al., 2018) instead of the latitudinal extent of continental ice  
194 sheets. However, such  $p\text{CO}_2$  proxies are potentially problematic as they can be difficult to  
195 calibrate in deep time and can be affected by secondary alteration. Even when stringent quality

196 criteria and the latest understanding of each of the  $p\text{CO}_2$  proxies have been applied to available  
197  $p\text{CO}_2$  records (Foster et al., 2017), both significant uncertainty in the estimated  $p\text{CO}_2$  for any  
198 given data point as well as disagreement between techniques remain (Fig. 4E). For instance, in  
199 the Late Triassic (~240-200 Ma), estimates of  $p\text{CO}_2$  span ~3000 ppm. Even a probabilistic  
200 approach to a large  $p\text{CO}_2$  proxy data set can not constrain  $p\text{CO}_2$  at the 95% confidence level to  
201 within a few hundred ppm for any given time interval, especially when we look deeper in time  
202 than the Cenozoic (Foster et al., 2017; Fig. 4E). For the pedogenic carbonate  $\delta^{13}\text{C}$  proxy, which  
203 forms the majority of the pre-Cenozoic data in the compilation of Foster et al. (2017), such  
204 scatter could result from diagenesis (Michel et al., 2016) and the sensitivity of the  $p\text{CO}_2$  estimates  
205 on assumptions regarding soil-respired CO<sub>2</sub> (Montañez, 2013). Nevertheless, despite these  
206 shortcomings, the  $p\text{CO}_2$  proxy record is broadly consistent with the ice extent record (Fig. 4E) -  
207  $p\text{CO}_2$  proxy data decreases ~400-310 Ma as the Late Devonian glacial interval occurs and the  
208 Permo-Carboniferous glacial interval begins and waxes,  $p\text{CO}_2$  proxy data roughly increases  
209 ~310-240 Ma as the Permo-Carboniferous glacial interval wanes and ends,  $p\text{CO}_2$  proxy data  
210 broadly remains relatively high ~240-40 Ma when no glacial intervals are robustly documented,  
211 and  $p\text{CO}_2$  proxy data roughly decreases ~40-0 Ma as the Cenozoic glacial interval begins. Given  
212 these considerations, we thus prefer to use the latitudinal extent of land ice to reflect Earth's  
213 overall climate state throughout the Phanerozoic, despite its own limitations.

## 214 RESULTS

215 In the ' $t_{1/2} = 36$  Myr' scenario, we observe four main peaks in the calculated LIP area within the  
216 tropics (Fig. 4C). The first peak ca. 510 Ma is associated with the emplacement of the  
217 Kalkarindji LIP, the second peak ca. 380 Ma is associated with the emplacement of the  
218 Kola-Dnieper LIP, the third peak ca. 200 Ma is associated with the emplacement of the Central  
219 Atlantic Magmatic Province (CAMP), and the fourth peak is associated with both the ca. 30 Ma  
220 emplacement of the Afar LIP as well as the earlier drift of the ca. 66 Ma Deccan LIP into the

tropics (Figs. 4A and 5). When we account for burial (' $t_{1/2} = 36 \text{ Myr} + 50\% \text{ burial}$ ' and ' $t_{1/2} = 36 \text{ Myr} + 100\% \text{ burial}$ ' scenarios), only the latter two of these four peaks are affected – the ca. 200 Ma peak is attenuated/removed due to the partial/complete burial of the CAMP, and the Cenozoic peak is attenuated due to the partial/complete burial of the Afar LIP. However, after accounting for burial, a minor area of LIPs remain in the tropics from ca. 130 Ma onwards, due to the Equatorial Atlantic Magmatic Province (EQUAMP), Caribbean-Colombian, and Deccan LIPs. Using the longer decay half-life of 120 Myr (the ' $t_{1/2} = 120 \text{ Myr} + 100\% \text{ burial}$ ' scenario) increases the area of LIPs in the tropics at any given time step, and has the effect of extending the duration of each peak.

The only scenario which results in a non-negative Pearson correlation coefficient (0.10) between LIP area in the tropics ( $\pm 15^\circ$ ; Fig. 4C) and the ice extent record (Fig. 4E) is the scenario with the slow decay rate and complete burial of LIPs associated with rifting (the ' $t_{1/2} = 120 \text{ Myr} + 100\% \text{ burial}$ ' scenario; Fig. 6). All other scenarios (including both total LIP area and tropical LIP area) yield a near zero or weak negative correlation coefficient (Fig. 6). The weak positive correlation of the ' $t_{1/2} = 120 \text{ Myr} + 100\% \text{ burial}$ ' scenario relative to the other scenarios can be primarily attributed to the complete removal of the CAMP, which was emplaced during an extended interval of ice-free conditions, as well as the effect of the longer decay half-life extending the duration of the earlier two peaks, such that they overlap more with the Late Ordovician and Permo-Carboniferous glacial intervals.

To assess the statistical significance of the correlation implied by the Pearson correlation coefficients (or lack thereof), we applied the approach of Macdonald et al. (2019) and simulated the four glacial episodes (Fig. 4E) occurring at random times through the past 520 Myr, and recomputed the correlation coefficient and % overlap between the LIP area in the tropics and the randomly timed glacial intervals for each of these 100,000 simulations (Fig. 6). This approach accounts for the fact that spurious correlation can arise between auto-correlated data sets such as these, where each value is not independent, but is instead dependent on the previous state of the

system. For the ' $t_{1/2} = 120$  Myr + 100% burial' scenario, 72% of the randomly timed glacial interval simulations correlate better with LIP area in the tropics than the actual ice extent record. With an associated p-value of 0.72, the null hypothesis that glacial intervals do not correlate to LIP area in the tropics cannot be rejected. Taking this approach, none of the positive or negative correlations that emerge between the LIP area scenarios and the ice extent record are statistically significant (Table 2).

## DISCUSSION

In the original models that proposed the 'Fire and Ice' hypothesis as an explanation for the onset of the Sturtian 'Snowball Earth' glaciation, chemical weathering was modeled as a function of temperature and runoff only (Donnadieu et al., 2004b). However, such an approach neglects the effects of soil shielding and regolith development in low-relief regions. Recent progress on understanding the relationships between landscapes, topography, and chemical weathering reveals that these effects are important (Gabet and Mudd, 2009; Hartmann et al., 2014; Maher and Chamberlain, 2014; Goddériss et al., 2017a). Soil shielding can lead to a transport-limited weathering regime in which the weathering rate of the underlying bedrock becomes insensitive to kinetic and equilibrium factors such as temperature and runoff - factors that would, in the absence of soil shielding, lead to relatively high weathering rates in the tropical rain belt. As a result, more recent modeling of chemical weathering incorporates such processes and highlights the importance of high-relief regions relative to low-relief ones for setting global weatherability (West, 2012; Goddériss et al., 2017a). LIPs are often emplaced in relatively low-relief areas, and as such, without active uplift, soil shielding from regolith development on these low-relief LIPs could significantly decrease the local weatherability of a LIP and mute its impact on global weatherability (as suggested in Kent and Muttoni, 2013). In this way, soil shielding could explain the lack of correlation between tropical LIP area and ice extent (Figs. 4 and 6). In contrast, processes that lead to continued exhumation of mafic lithologies and the creation of steep

272 topography that minimizes soil shielding, particularly in tropical regions, may exert a strong  
273 control on global weatherability and long-term climate. This interpretation underlies the  
274 hypothesis that arc-continent collisions in the tropics during the Ordovician (Swanson-Hysell and  
275 Macdonald, 2017) and the Cenozoic (Jagoutz et al., 2016) played a significant role in transitions  
276 into glacial climate states at those times - a correlation that appears robust throughout the  
277 Phanerozoic (Macdonald et al., 2019).

278 A complication with the interpretation of soil shielding and limited weathering of LIPs is the  
279 rapid area decay rate ( $t_{1/2} = 36$  Myr) inferred from the comparison of current LIP surface extent  
280 to estimated original surface extent (Fig. 2). A couple considerations are relevant with respect to  
281 this analysis: 1) the current surface extent of LIP exposure is reduced in part by volcanics being  
282 covered by unconsolidated sediments (i.e. regolith development itself) in a number of the  
283 provinces; 2) the current surface extent of LIP exposure may be incomplete and an underestimate  
284 for some of the provinces; 3) the initial LIP surface extents are typically poorly constrained and  
285 are likely over-estimates which could be resulting in inflated interpreted decay rates; and 4) the  
286 relationship between LIP area and volume is poorly constrained. Future efforts that improve the  
287 LIP database, such as developing better-constrained estimates of original LIP surface extent,  
288 constraining burial and uplift histories, and refining the timing of eruptions associated with LIPs,  
289 will improve analyses that consider the LIP record in its entirety, such as that in this contribution.

290 We have focused this analysis on the Phanerozoic record given that well-constrained  
291 paleogeographic models are available for the past  $\sim 520$  Myr. The approach of seeking to evaluate  
292 correlation between LIP area and glaciation is further complicated for Neoproterozoic Snowball  
293 Earth events because ice-albedo runaway leads to persistent global glaciation on timescales of tens  
294 of millions of years without continued forcing through normal carbon cycle processes until  
295 sufficient CO<sub>2</sub> to drive deglaciation builds up in the absence of silicate weathering (Hoffman  
296 et al., 2017). Moreover, cooling past the critical threshold for rapid global glaciation may have  
297 occurred on a sub-million year timescale (e.g. Macdonald and Wordsworth, 2017). Nevertheless,

298 evaluating the hypothesis of tropical LIP area associated with the ca. 720 Ma Franklin LIP  
299 increasing global weatherability and contributing to the onset of the Sturtian Snowball Earth is a  
300 major motivating driver behind conducting this analysis.

301 How does the tropical LIP area associated with the Franklin LIP compare to that observed in  
302 the Phanerozoic? Using the paleomagnetic pole of Denyszyn et al. (2009), we reconstruct the  
303 paleolatitude of the Franklin LIP at the time of emplacement, and find that ~99.7% (or  
304 ~2.6 Mm<sup>2</sup>) of the LIP erupted within 15° of the equator. This Franklin LIP tropical area at the  
305 time of emplacement is approximately equivalent to the Cenozoic peak, and is smaller than the  
306 other Phanerozoic peaks (Fig. 4C). The ca. 1109 Ma Umkondo is another Precambrian LIP that  
307 is constrained to have erupted in the tropics, although it is not known to be associated with any  
308 glaciation (no glacial deposits are found within the contemporaneous Midcontinent Rift basin;  
309 Swanson-Hysell et al., 2019). We reconstruct the paleolatitude of the Umkondo LIP at the time of  
310 emplacement using the paleomagnetic pole of Swanson-Hysell et al. (2015), and find that  
311 effectively all of the LIP (or ~2.0 Mm<sup>2</sup>) erupted within the tropics, an area that is slightly  
312 smaller than that estimated for the Franklin LIP (Fig. 4C).

313 Together, these results indicate that the Franklin LIP, when compared to Phanerozoic as well  
314 as other Precambrian LIPs, did not have a uniquely large area in the tropics. Given that similar  
315 (and larger) peaks in tropical LIP area are not associated with the onset of glacial periods,  
316 additional processes beyond an increase in weatherability due to LIP area in the tropics must  
317 have been at play in the initiation of the Sturtian Snowball Earth. One such process could have  
318 been unusually high planetary albedo associated with the low-latitude continental configuration of  
319 the supercontinent Rodinia (Kirschvink, 1992; Li et al., 2008). However, our analysis of zonal  
320 continental area reveals an almost invariant tropical continental area from ~400 Ma to the  
321 present (Fig. 7) and consequently no significant correlation between tropical continental area and  
322 the ice extent record in the Phanerozoic, although it is intriguing that there is a high and rising  
323 low-latitude continental area in the Ordovician. Similar to the LIP area analysis, this continental

area analysis suggests that a low-latitude continental configuration can not be invoked as the sole driver of planetary cooling, although it could be a contributing factor. Another potential contributing process for Neoproterozoic cooling leading up to the Sturtian glaciation is an increase in global weatherability associated with the collision and accretion of arc terranes within the present-day Arabian-Nubian Shield (Park et al., in review). Together, a low-latitude continental configuration and abundant arc-continent collisions in the tropics may have led to a cool background climate, and the emplacement of the Franklin LIP may have further increased global weatherability to the point where the ice-albedo runaway could take effect. However, tropical LIP area associated with the Franklin was not uniquely high, and therefore an associated increase in global weatherability was likely not the sole driver of Snowball Earth onset, consistent with the results of the Phanerozoic analysis.

The temporal overlap between Franklin LIP eruptions and the initiation of Sturtian glaciation remains compelling (Macdonald et al., 2010; MacLennan et al., 2018). This overlap could support arguments that other aspects of LIP emplacement, such as the injection of sulfur aerosols in the stratosphere (Macdonald and Wordsworth, 2017), played a role in the initiation of low-latitude glaciation. The temporary effect on albedo of such aerosols is maximized when they are injected into the atmosphere at low-latitudes into a cool background climate and their presence at high concentrations is pre-conditioned on eruption through sedimentary basins hosting evaporite deposits, as could have been the case for the Franklin LIP (Macdonald and Wordsworth, 2017). However, in the cases in which such aerosol-driven cooling does not result in ice-albedo runaway and a Snowball Earth, the climate would return to its background climate state within years (Macdonald and Wordsworth, 2017). A contrasting effect is that, on 1 kyr to 1 Myr timescales, LIP emplacement could instead cause transient warming associated with elevated CO<sub>2</sub> outgassing leading to transiently high pCO<sub>2</sub>, as has been argued for the CAMP (Schaller et al., 2011, 2012).

The results from this analysis indicate that when the entire LIP database is considered in conjunction with a paleogeographic reconstruction and this parameterization of erosion, there is

350 no significant relationship between total LIP area nor LIP area in the tropics and the extent of  
351 continental ice sheets. While this result need not imply that there is no increase in global  
352 weatherability from the emplacement of LIPs, it does suggest that changes in planetary  
353 weatherability associated with LIPs are not the fundamental control on whether Earth is in a  
354 glacial or non-glacial climate state.

## 355 ACKNOWLEDGEMENTS

356 Richard Ernst provided GIS compilations of LIP extent and present-day exposure that were  
357 essential to the analysis. Discussions with Yves Goddériss made possible through the  
358 France-Berkeley Fund contributed valuably to aspects of the interpretation. Park was supported  
359 by NSF Grant 1547434 awarded to Swanson-Hysell.

360 **TABLES**

**Table 1.** Phanerozoic large igneous provinces (and the Franklin).

name	age (Ma)	age ref.	original <sup>1</sup> area (Mm <sup>2</sup> )	present <sup>2</sup> area (Mm <sup>2</sup> )	present area ref.	present <sup>3</sup> / original	half-life <sup>4</sup> (Myr)	buried?
Columbia River	16	Kasbohm and Schoene (2018)	0.68	0.38	Buchan and Ernst (2004)	0.56	19.2	no
Afar	30	Courtillot and Renne (2003)	2.05	0.63	Coffin et al. (2006)	0.31	17.7	partial
NAIP	62	Larsen et al. (2015)	1.07	0.29	Buchan and Ernst (2004); Coffin et al. (2006)	0.27	33.0	partial
Deccan	66	Schoene et al. (2014)	0.83	0.56	Coffin et al. (2006)	0.68	116.6	no
Seychelles	66	Schoene et al. (2014)	0.46	0.00	Coffin et al. (2006)	0.00	0.0	yes
Madagascar	90	Cucciniello (2010)	0.63	0.03	Coffin et al. (2006)	0.05	20.8	no
Caribbean-Colombian	94	Loewen et al. (2013)	0.71	0.13	Coffin et al. (2006)	0.18	37.6	no
HALIP	95	Kingsbury et al. (2018)	3.60	0.15	Hartmann and Moosdorf (2012)	0.04	20.7	no
EQUAMP	131	Hollanda et al. (2016)	0.66	0.01	Hollanda et al. (2016)	0.01	20.5	no
Comei	132	Zhu et al. (2009)	0.11	-	-	-	-	no
Bunbury	132	Zhu et al. (2009)	0.03	0.00	Thorne et al. (2014)	0.05	30.9	no
Parana-Etendeka	135	Florisbal et al. (2014); Almeida et al. (2018)	3.12	0.40	Coffin et al. (2006)	0.13	45.7	partial
Trap	140	Ernst and Buchan (2001)	0.03	0.00	Ernst and Buchan (2001)	0.00	0.0	no
NW Australia Margin	160	Pirajno and Hoatson (2012)	0.62	0.00	Coffin et al. (2006)	0.00	0.0	yes
Karoo	183	Burgess et al. (2015)	3.21	0.15	de Kock compilation <sup>5</sup>	0.05	41.3	no
Ferrar	183	Burgess et al. (2015)	0.18	-	-	-	-	no
CAMP	201	Blackburn et al. (2013)	11.46	0.23	Marzoli and Parisio compilation <sup>6</sup>	0.02	35.7	partial
Siberia	252	Burgess and Bowring (2015)	3.46	0.47	Coffin et al. (2006)	0.14	87.5	no
Emeishan	259	Zhou et al. (2002)	0.71	0.06	Coffin et al. (2006)	0.09	72.9	no
Panjal-Qiangtang	283	Zhai et al. (2013)	0.11	-	-	-	-	no
Tarim	290	Xu et al. (2014)	0.35	-	-	-	-	no
Magdalen	360	Murphy et al. (1999)	0.42	-	-	-	-	no
Vilyui	374	Ricci et al. (2013)	1.14	-	-	-	-	no
Kola-Dnieper	380	Arzamastsev and Wu (2014)	5.90	-	-	-	-	no
Suordakh	450	Khudoley et al. (2013)	0.02	-	-	-	-	no
Kalkarindji	511	Jourdan et al. (2014)	3.54	0.17	Thorne et al. (2014)	0.05	116.3	no
Franklin	720	Denyszyn et al. (2009)	2.62	0.04	Buchan and Ernst (2004)	0.02	121.8	no

<sup>1</sup>obtained via calculating the area of the continental portions of polygons within the LIP original surface extent compilation of Ernst and Youbi (2017) and Ernst (2019), shown as blue polygons in Fig. 1.

<sup>2</sup>obtained via calculating the area of polygons from the noted reference of presently-exposed volcanics associated with LIPs, shown as orange polygons in Fig. 1.

<sup>3</sup>present area / original area

<sup>4</sup>assuming exponential decay with form  $N(t) = 2^{t/t_{1/2}}$ .

<sup>5</sup>from ArcGIS compilation produced by M. de Kock for the LIPs Reconstruction Project (Ernst et al., 2013).

<sup>6</sup>from ArcGIS compilation produced by A. Marzoli and L. Parisio for the LIPs Reconstruction Project (Ernst et al., 2013).

**Table 2.** Statistics of correlation between large igneous province area and ice extent.

scenario	within tropics $\pm 15^\circ$				total <sup>5</sup>				within tropics $\pm 10^\circ$				within tropics $\pm 20^\circ$			
	correlation <sup>1</sup> val. <sup>3</sup>	p-val. <sup>4</sup>	% overlap <sup>2</sup> val.	p-val.	correlation val.	p-val.	% overlap val.	p-val.	correlation val.	p-val.	% overlap val.	p-val.	correlation val.	p-val.	% overlap val.	p-val.
$t_{1/2} = 36$ Myr	-0.19	0.81	13	0.94	-0.26	0.85	30	0.95	-0.22	0.86	13	0.95	-0.17	0.77	9	0.96
$t_{1/2} = 36$ Myr + 50% burial	-0.14	0.73	22	0.85	-0.25	0.84	52	0.97	-0.17	0.79	9	0.90	-0.10	0.67	26	0.86
$t_{1/2} = 36$ Myr + 100% burial	-0.02	0.45	22	0.65	-0.14	0.74	65	0.94	-0.08	0.54	9	0.76	0.04	0.37	22	0.65
$t_{1/2} = 120$ Myr + 100% burial	0.10	0.32	35	0.72	0.00	0.51	100	1.00	0.02	0.40	26	0.77	0.19	0.24	48	0.66

<sup>1</sup>Pearson correlation coefficient between LIP area and the actual ice extent record.

<sup>2</sup>% of time when both LIP area is >30% of the maximum and ice extent is > $10^\circ$  from the poles.

<sup>3</sup>'val.' refers to the computed correlation coefficient/% overlap between LIP area and the actual ice extent record.

<sup>4</sup>'p-val.' refers to the fraction of randomly timed glacial interval simulations that correlate/overlap better with LIP area than the actual ice extent record (i.e. the p-value with respect to the null hypothesis of no correlation/overlap). P-values <0.05 indicate that we can reject the null hypothesis at the 95% confidence level.

<sup>5</sup>all latitudes.

<sup>361</sup> **FIGURES**

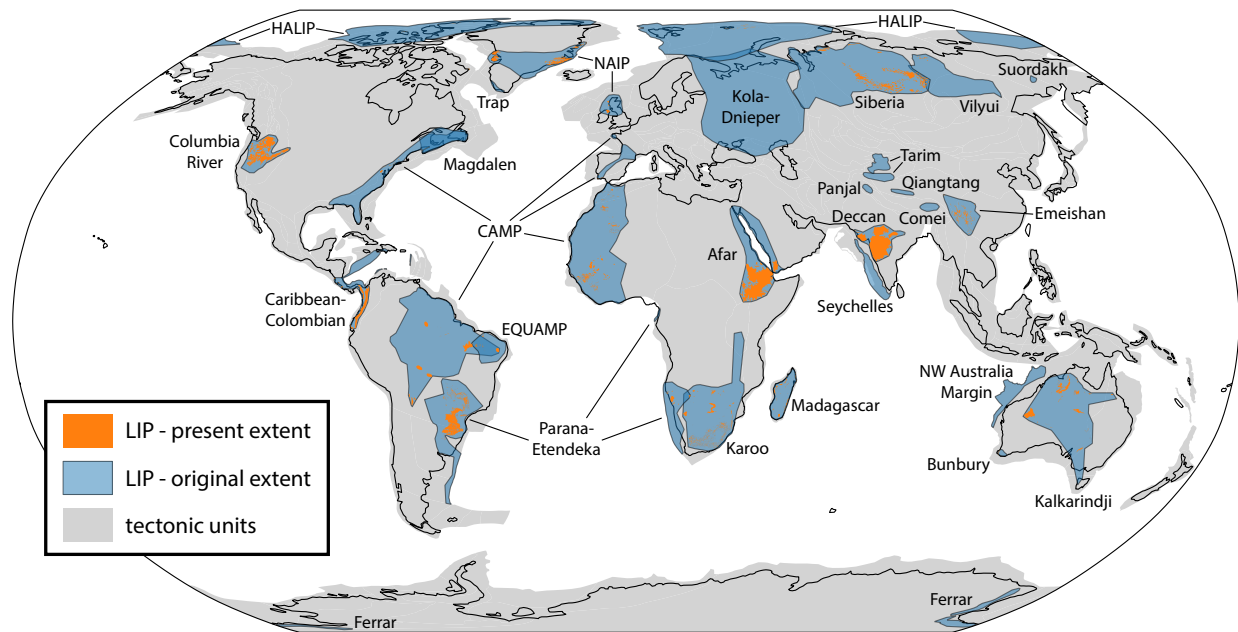


**Figure 1.** Map of current surface extent of volcanic lithologies associated with LIPs that erupted between 520 Ma and the present, as well as the estimates of the initial LIP surface extent used in the area analysis (modified slightly from Ernst and Youbi, 2017 and Ernst, 2019 to ensure that all currently exposed volcanic lithologies are encapsulated by the initial LIP surface area polygons).

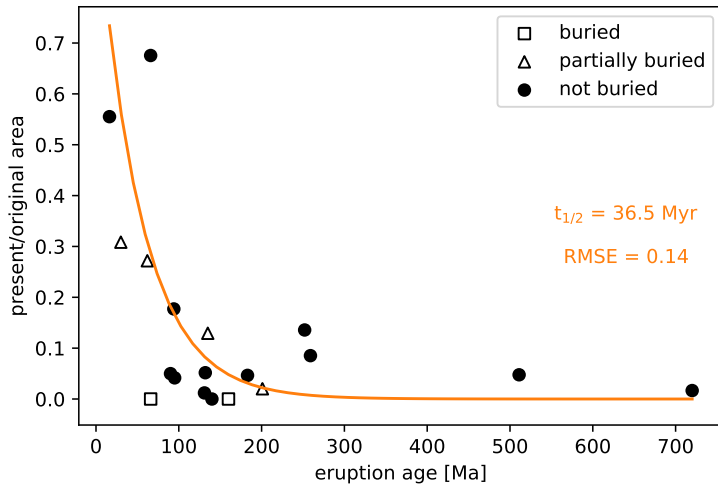


**Figure 2.** LIP erosion through time. The ratio of estimates of the present-day surface area to that of the original surface area are shown for 19 basaltic LIPs. An exponential fit is made to the 13 basaltic LIPs that are interpreted to not have been buried after emplacement (Table 1), which yields a half-life of  $\sim 36$  Myr. RMSE = root mean square error.

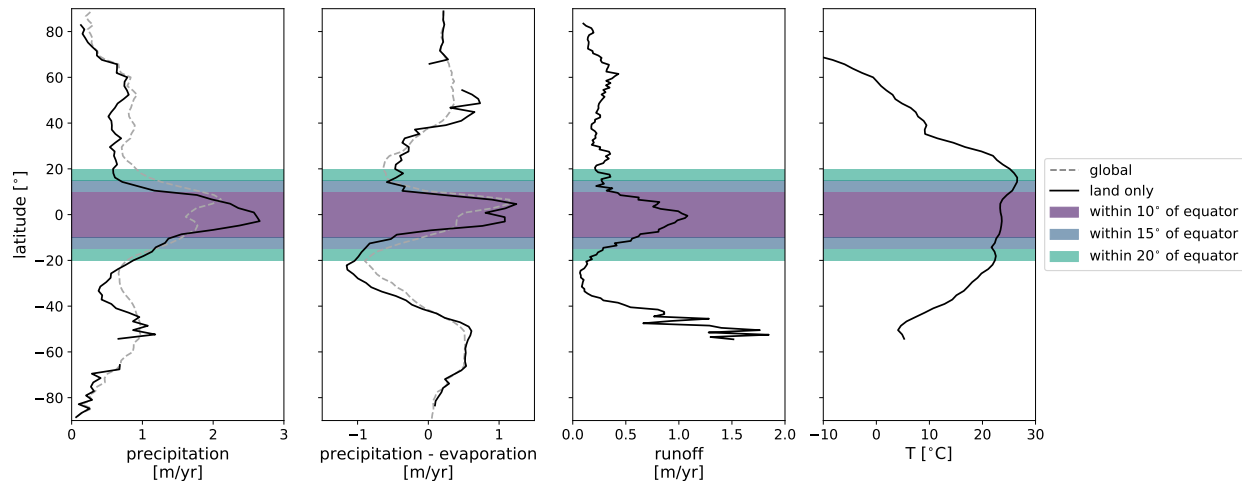


**Figure 3.** Zonally averaged modern climatological data used to define the tropical rain belt. The global precipitation (Kalnay et al., 1996) and precipitation minus evaporation (Trenberth et al., 2011) data include land and ocean pixels, global temperature data (Kalnay et al., 1996) are from land only, and runoff data (Fekete et al., 1999) are from land only excluding Antarctica. The peak in runoff  $\sim 50^\circ$  is due to anomalously high orographically-induced runoff in the southern Andes, which represents almost all of the land in that latitude belt. Temperature data for Antarctica are off scale. Precipitation, precipitation minus evaporation, and runoff all increase sharply between  $\pm 10^\circ$  and  $\pm 15^\circ$ .

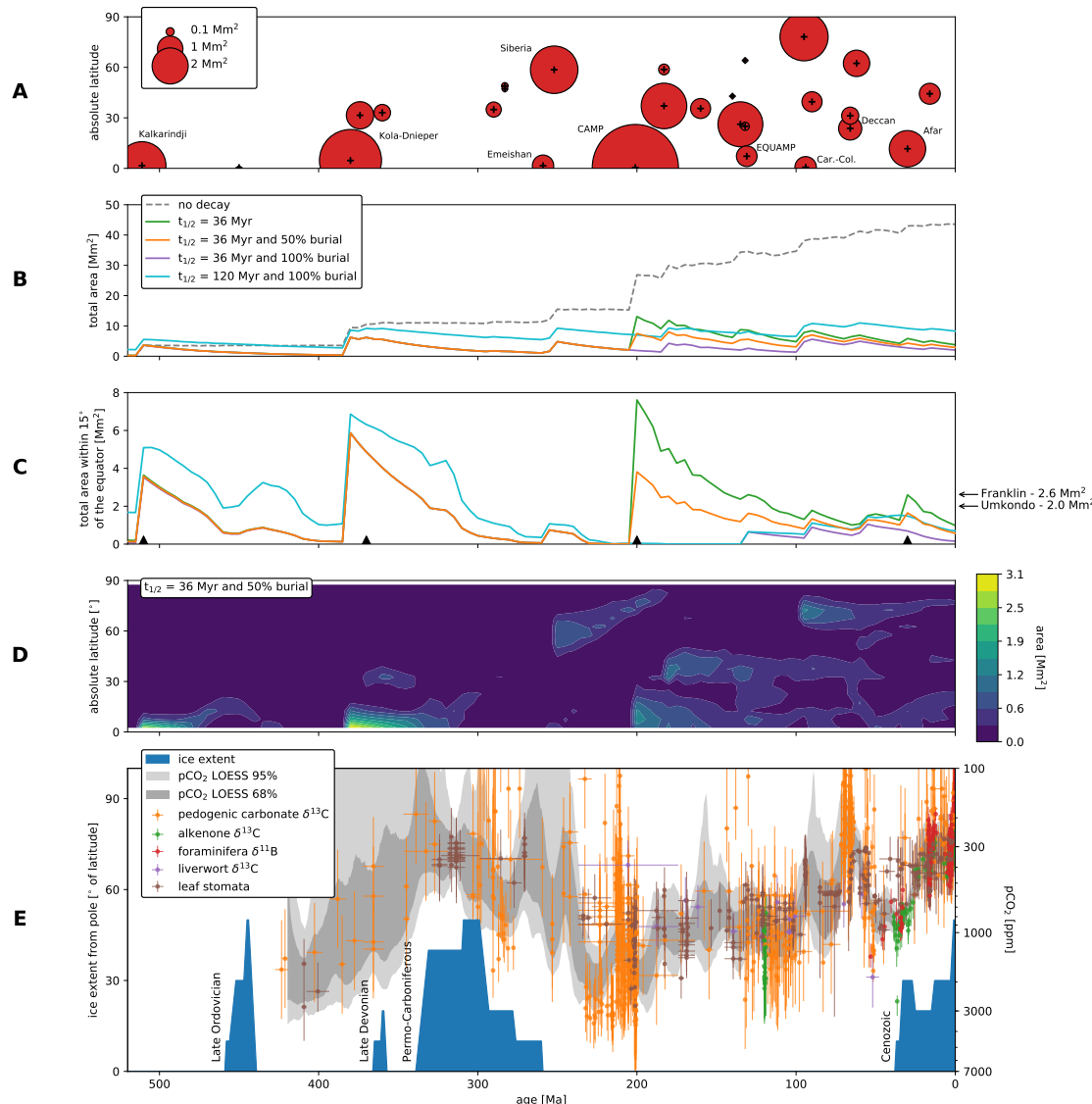


**Figure 4.** **A)** LIPs included in this analysis. The size of each circle reflects the initial surface area estimate of each LIP. The + indicates the timing and absolute paleolatitude of the centroid of each LIP at the time of emplacement. Car.-Col. = Caribbean-Colombian. **B)** Total LIP area through time for the different post-emplacement scenarios. Only the ‘no decay’ scenario excludes pre-Phanerozoic LIPs. **C)** Tropical LIP area through time for the different post-emplacement scenarios. The arrows to the right indicate reconstructed tropical LIP area at the time of emplacement for the ca. 720 and 1109 Ma Franklin and Umkondo LIPs. The triangles show the paleogeographic reconstruction times in Fig. 5. **D)** Contour plot showing the latitudinal distribution of LIP area for one of the post-emplacement models. **E)** Latitudinal extent of land ice away from the poles (Macdonald et al., 2019) and compilation of  $p\text{CO}_2$  proxies (Foster et al., 2017) ( $p\text{CO}_2$  y-axis reversed, and in log-scale). Error bars indicate standardized uncertainties, and grey bands indicate 68 and 95% confidence intervals for Monte Carlo resampled LOESS fits to the  $p\text{CO}_2$  proxy data (Foster et al., 2017). Note that there are  $p\text{CO}_2$  proxy estimates <100 ppm that are cut off in this plot.

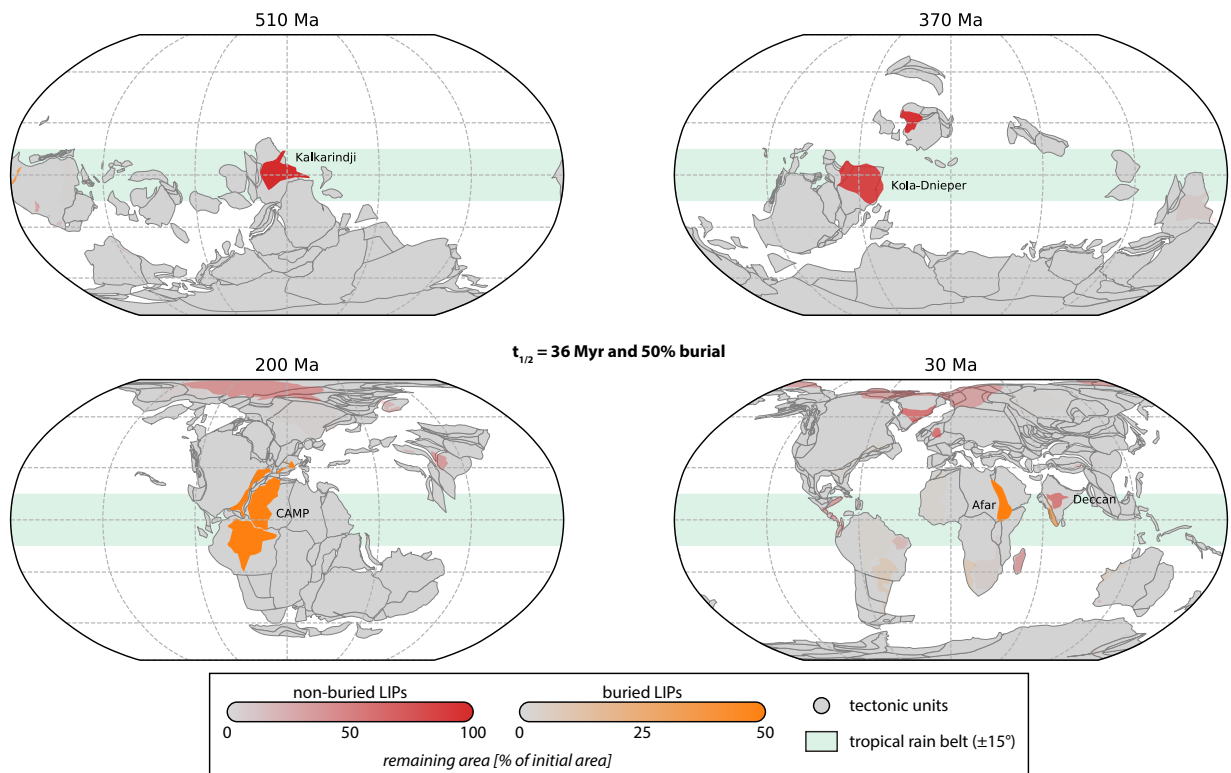


**Figure 5.** Paleogeographic reconstructions for times that correspond to peaks of LIP area in the tropics (Fig. 4C). The opacity of LIP polygons indicates their parameterized remaining area at the time of the reconstruction as a percentage of initial LIP area, under the preferred post-emplacement scenario of ' $t_{1/2} = 36 \text{ Myr} + 50\% \text{ burial}$ '.

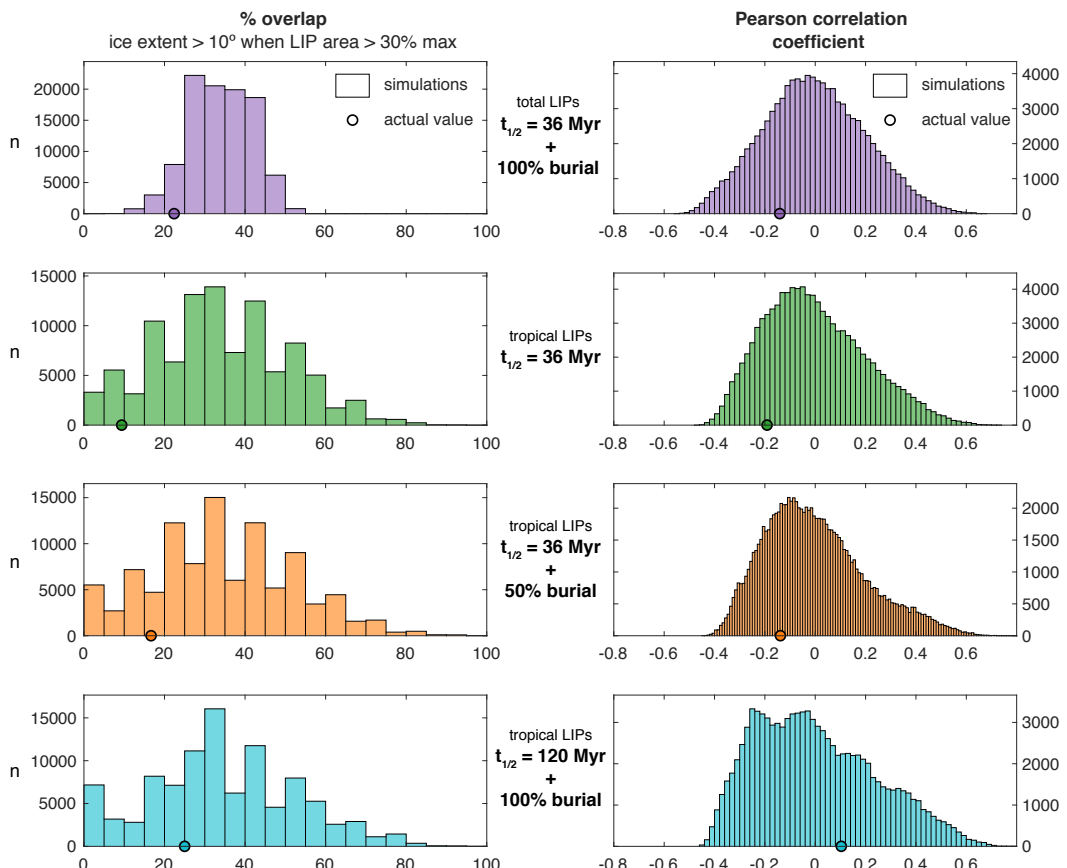


**Figure 6.** The % overlap and Pearson correlation coefficients between LIP area and the actual ice-extent record are shown with circles. These values are compared to histograms that show the range of values that arise when comparing the LIP area record to glacial intervals that have been shifted randomly in time 100,000 times. The fraction of randomly timed glacial interval simulations that correlate/overlap better with LIP area than the actual ice-extent record is the p-value shown in Table 2.

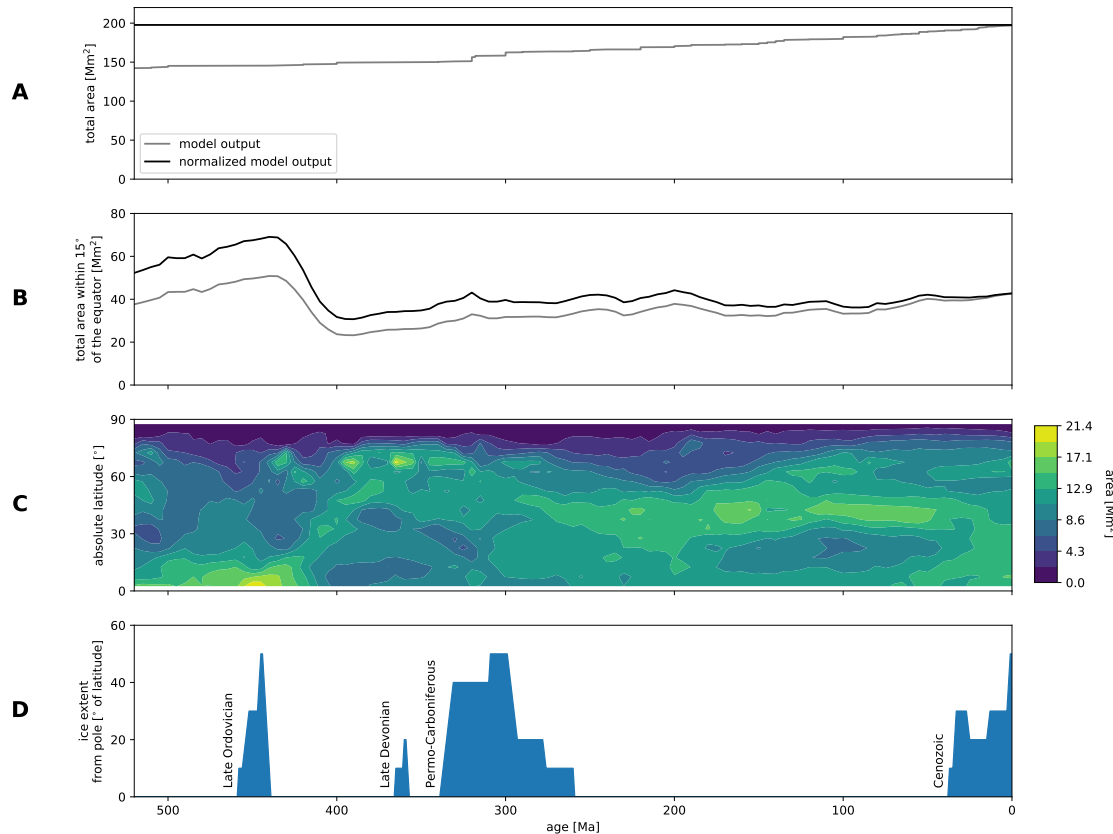


**Figure 7.** **A)** Total continental area through time. In the paleogeographic model used in this study, tectonic units (Torsvik and Cocks, 2016) are progressively added to the model, leading to a net increase in total continental area in the model of  $\sim 33\%$  over the Phanerozoic. However, estimates of continental crust growth (e.g. Pujol et al., 2013) suggest that continental area was roughly constant through the Phanerozoic. We therefore normalize the total continental area curve in our model by assuming a fixed continental area through the Phanerozoic. **B)** Tropical continental area through time. We normalize the tropical continental area curve using the normalization ratio implied in (A). **C)** Contour plot showing the latitudinal distribution of continental area. **D)** Latitudinal extent of land ice away from the poles (Macdonald et al., 2019).

## 362 References

- 363 Almeida, V. V., Janasi, V. A., Heaman, L. M., Shaulis, B. J., Hollanda, M. H. B., and Renne, P. R., 2018,  
364 Contemporaneous alkaline and tholeiitic magmatism in the Ponta Grossa Arch, Paraná-Etendeka Magmatic  
365 Province: Constraints from U-Pb zircon/baddeleyite and  $^{40}\text{Ar}/^{39}\text{Ar}$  phlogopite dating of the José Fernandes  
366 Gabbro and mafic dykes: Journal of Volcanology and Geothermal Research, vol. 355, pp. 55–65,  
367 doi:10.1016/j.jvolgeores.2017.01.018.
- 368 Arzamastsev, A. A. and Wu, F.-Y., 2014, U-Pb geochronology and Sr-Nd isotopic systematics of minerals from the  
369 ultrabasic-alkaline massifs of the Kola province: Petrology, vol. 22, pp. 462–479, doi:10.1134/s0869591114050026.
- 370 Blackburn, T. J., Olsen, P. E., Bowring, S. A., McLean, N. M., Kent, D. V., Puffer, J., McHone, G., Rasbury, E. T.,  
371 and Et-Touhami, M., 2013, Zircon U-Pb geochronology links the End-Triassic extinction with the Central  
372 Atlantic Magmatic Province: Science, vol. 340, pp. 941–945, doi:10.1126/science.1234204.
- 373 Boucot, A. J., Xu, C., Scotese, C. R., and Morley, R. J., 2013, Phanerozoic Paleoclimate: An Atlas of Lithologic  
374 Indicators of Climate: SEPM (Society for Sedimentary Geology), doi:10.2110/sepmcsp.11.
- 375 Buchan, K. L. and Ernst, R. E., 2004, Diabase dyke swarms and related units in Canada and adjacent regions:  
376 Geological Survey of Canada Map 2022A, doi:10.4095/214883.
- 377 Burgess, S. D. and Bowring, S. A., 2015, High-precision geochronology confirms voluminous magmatism before,  
378 during, and after Earth's most severe extinction: Science Advances, vol. 1, pp. 1–14, doi:10.1126/sciadv.1500470.
- 379 Burgess, S. D., Bowring, S. A., Fleming, T. H., and Elliot, D. H., 2015, High-precision geochronology links the  
380 Ferrar large igneous province with early-Jurassic ocean anoxia and biotic crisis: Earth and Planetary Science  
381 Letters, vol. 415, pp. 90–99, doi:10.1016/j.epsl.2015.01.037.
- 382 Cao, W., Williams, S., Flament, N., Zahirovic, S., Scotese, C., and Müller, R. D., 2018, Palaeolatitudinal  
383 distribution of lithologic indicators of climate in a palaeogeographic framework: Geological Magazine, vol. 156,  
384 pp. 331–354, doi:10.1017/s0016756818000110.
- 385 Coffin, M., Duncan, R., Eldholm, O., Fitton, J. G., Frey, F., Larsen, H. C., Mahoney, J., Saunders, A., Schlich, R.,  
386 and Wallace, P., 2006, Large igneous provinces and scientific ocean drilling: Status quo and a look ahead:  
387 Oceanography, vol. 19, pp. 150–160, doi:10.5670/oceanog.2006.13.
- 388 Courtillot, V. E. and Renne, P. R., 2003, On the ages of flood basalt events: Comptes Rendus Geoscience, vol. 335,  
389 pp. 113–140, doi:10.1016/s1631-0713(03)00006-3.
- 390 Cox, G. M., Halverson, G. P., Stevenson, R. K., Vokaty, M., Poirier, A., Kunzmann, M., Li, Z.-X., Denyszyn, S. W.,  
391 Strauss, J. V., and Macdonald, F. A., 2016, Continental flood basalt weathering as a trigger for Neoproterozoic  
392 Snowball Earth: Earth and Planetary Science Letters, vol. 446, pp. 89–99, doi:10.1016/j.epsl.2016.04.016.
- 393 Cucciniello, C., 2010, U-Pb ages, Pb-Os isotope ratios, and platinum-group element (PGE) composition of the  
394 West-Central Madagascar flood basalt province: The Journal of Geology, vol. 118, pp. 523–541,  
395 doi:10.1086/655012.
- 396 DeConto, R. M., Pollard, D., Wilson, P. A., Pälike, H., Lear, C. H., and Pagani, M., 2008, Thresholds for Cenozoic  
397 bipolar glaciation: Nature, vol. 455, pp. 652–656, doi:10.1038/nature07337.
- 398 Denyszyn, S. W., Halls, H. C., Davis, D. W., and Evans, D. A., 2009, Paleomagnetism and U-Pb geochronology of  
399 Franklin dykes in High Arctic Canada and Greenland: a revised age and paleomagnetic pole constraining block  
400 rotations in the Nares Strait region: Canadian Journal of Earth Sciences, vol. 46, pp. 689–705,  
401 doi:10.1139/E09-042.
- 402 Dessert, C., Dupré, B., Gaillardet, J., François, L. M., and Allègre, C. J., 2003, Basalt weathering laws and the  
403 impact of basalt weathering on the global carbon cycle: Chemical Geology, vol. 202, pp. 257–273,  
404 doi:10.1016/j.chemgeo.2002.10.001.

- 405 Domeier, M., 2018, Early Paleozoic tectonics of Asia: Towards a full-plate model: Geoscience Frontiers, vol. 9, pp.  
406 789–862, doi:10.1016/j.gsf.2017.11.012.
- 407 Donnadieu, Y., Godderis, Y., Ramstein, G., Nedelev, A., and Meert, J., 2004a, A ‘snowball Earth’ climate triggered  
408 by continental break-up through changes in runoff: Nature, vol. 428, pp. 303–306.
- 409 Donnadieu, Y., Ramstein, G., Fluteau, F., Roche, D., and Ganopolski, A., 2004b, The impact of atmospheric and  
410 oceanic heat transports on the sea-ice-albedo instability during the Neoproterozoic: Climate Dynamics, vol. 22,  
411 pp. 293–306, doi:10.1007/s00382-003-0378-5.
- 412 Donohoe, A. and Voigt, A., 2017, Why future shifts in tropical precipitation will likely be small: Geophysical  
413 Monograph Series, pp. 115–137, doi:10.1002/9781119068020.ch8.
- 414 Ernst, R. E., 2019, Introduction to environmental change and large igneous provinces: The deadly kiss of LIPs: In  
415 Environmental Change and Large Igneous Provinces: The Deadly Kiss of LIPs, American Geophysical Union.
- 416 Ernst, R. E., Bleeker, W., Söderlund, U., and Kerr, A. C., 2013, Large igneous provinces and supercontinents:  
417 Toward completing the plate tectonic revolution: Lithos, vol. 174, pp. 1–14, doi:10.1016/j.lithos.2013.02.017.
- 418 Ernst, R. E. and Buchan, K. L., 2001, Large mafic magmatic events through time and links to mantle-plume heads:  
419 In Special Paper 352: Mantle plumes: their identification through time, Geological Society of America, pp.  
420 483–575, doi:10.1130/0-8137-2352-3.483.
- 421 Ernst, R. E. and Youbi, N., 2017, How large igneous provinces affect global climate, sometimes cause mass  
422 extinctions, and represent natural markers in the geological record: Palaeogeography, Palaeoclimatology,  
423 Palaeoecology, vol. 478, pp. 30–52, doi:10.1016/j.palaeo.2017.03.014.
- 424 Evans, D. A. D., 2006, Proterozoic low orbital obliquity and axial-dipolar geomagnetic field from evaporite  
425 palaeolatitudes: Nature, vol. 444, pp. 51–55, doi:10.1038/nature05203.
- 426 Fekete, B. M., Vörösmarty, C. J., and Grabs, W., 1999, Global, composite runoff fields based on observed river  
427 discharge and simulated water balances: Global Runoff Data Centre Koblenz, Germany.
- 428 Florisbal, L. M., Heaman, L. M., de Assis Janasi, V., and de Fatima Bitencourt, M., 2014, Tectonic significance of  
429 the Florianópolis Dyke Swarm, Paraná-Etendeka Magmatic Province: A reappraisal based on precise U-Pb  
430 dating: Journal of Volcanology and Geothermal Research, vol. 289, pp. 140–150,  
431 doi:10.1016/j.jvolgeores.2014.11.007.
- 432 Foster, G. L., Royer, D. L., and Lunt, D. J., 2017, Future climate forcing potentially without precedent in the last  
433 420 million years: Nature Communications, vol. 8, p. 14,845, doi:10.1038/ncomms14845.
- 434 Gabet, E. J. and Mudd, S. M., 2009, A theoretical model coupling chemical weathering rates with denudation rates:  
435 Geology, vol. 37, pp. 151–154, doi:10.1130/G25270A.1.
- 436 Gislason, S. R. and Oelkers, E. H., 2003, Mechanism, rates, and consequences of basaltic glass dissolution: II. an  
437 experimental study of the dissolution rates of basaltic glass as a function of pH and temperature: Geochimica et  
438 Cosmochimica Acta, vol. 67, pp. 3817–3832, doi:10.1016/s0016-7037(03)00176-5.
- 439 Goddérés, Y., Donnadieu, Y., Carretier, S., Aretz, M., Dera, G., Macouin, M., and Regard, V., 2017a, Onset and  
440 ending of the late Palaeozoic ice age triggered by tectonically paced rock weathering: Nature Geoscience, vol. 10,  
441 pp. 382–386, doi:10.1038/ngeo2931.
- 442 Goddérés, Y., Hir, G. L., Macouin, M., Donnadieu, Y., Hubert-Théou, L., Dera, G., Aretz, M., Fluteau, F., Li,  
443 Z. X., and Halverson, G. P., 2017b, Paleogeographic forcing of the strontium isotopic cycle in the Neoproterozoic:  
444 Gondwana Research, vol. 42, pp. 151–162, doi:10.1016/j.gr.2016.09.013.

- 445 Hartmann, J., Jansen, N., Dürr, H. H., Kempe, S., and Köhler, P., 2009, Global CO<sub>2</sub>-consumption by chemical  
446 weathering: What is the contribution of highly active weathering regions?: *Global and Planetary Change*,  
447 vol. 69, pp. 185–194, doi:10.1016/j.gloplacha.2009.07.007.
- 448 Hartmann, J. and Moosdorf, N., 2012, The new global lithological map database GLiM: A representation of rock  
449 properties at the Earth surface: *Geochemistry, Geophysics, Geosystems*, vol. 13, doi:10.1029/2012GC004370.
- 450 Hartmann, J., Moosdorf, N., Lauerwald, R., Hinderer, M., and West, A. J., 2014, Global chemical weathering and  
451 associated P-release - the role of lithology, temperature and soil properties: *Chemical Geology*, vol. 363, pp.  
452 145–163, doi:10.1016/j.chemgeo.2013.10.025.
- 453 Hoffman, P. F., Abbot, D. S., Ashkenazy, Y., Benn, D. I., Brocks, J. J., Cohen, P. A., Cox, G. M., Creveling, J. R.,  
454 Donnadieu, Y., Erwin, D. H., Fairchild, I. J., Ferreira, D., Goodman, J. C., Halverson, G. P., Jansen, M. F.,  
455 Le Hir, G., Love, G. D., Macdonald, F. A., Maloof, A. C., Partin, C. A., Ramstein, G., Rose, B. E. J., Rose,  
456 C. V., Sadler, P. M., Tziperman, E., Voigt, A., and Warren, S. G., 2017, Snowball Earth climate dynamics and  
457 Cryogenian geology-geobiology: *Science Advances*, vol. 3, doi:10.1126/sciadv.1600983.
- 458 Hollanda, M. H. B. M., Archanjo, C. J., Renne, P. R., Ngonge, D. E., Castro, D. L., Oliveira, D. C., and  
459 Macêdo Filho, A. A., 2016, Evidence of an Early Cretaceous giant dyke swarm in northeast Brazil (South  
460 America): A geodynamic overview: *Acta Geologica Sinica - English Edition*, vol. 90, pp. 109–110,  
461 doi:10.1111/1755-6724.12915.
- 462 Ibarra, D. E., Caves, J. K., Moon, S., Thomas, D. L., Hartmann, J., Chamberlain, C. P., and Maher, K., 2016,  
463 Differential weathering of basaltic and granitic catchments from concentration-discharge relationships:  
464 *Geochimica et Cosmochimica Acta*, vol. 190, pp. 265 – 293, doi:10.1016/j.gca.2016.07.006.
- 465 Jagoutz, O., Macdonald, F. A., and Royden, L., 2016, Low-latitude arc-continent collision as a driver for global  
466 cooling: *Proceedings of the National Academy of Sciences*, vol. 113, pp. 4935–4940, doi:10.1073/pnas.1523667113.
- 467 Johansson, L., Zahirovic, S., and Müller, R. D., 2018, The interplay between the eruption and weathering of large  
468 igneous provinces and the deeptime carbon cycle: *Geophysical Research Letters*, vol. 45,  
469 doi:10.1029/2017GL076691.
- 470 Jourdan, F., Hodges, K., Sell, B., Schaltegger, U., Wingate, M., Evins, L., Söderlund, U., Haines, P., Phillips, D.,  
471 and Blenkinsop, T., 2014, High-precision dating of the Kalkarindji large igneous province, Australia, and  
472 synchrony with the Early-Middle Cambrian (Stage 4-5) extinction: *Geology*, vol. 42, pp. 543–546,  
473 doi:10.1130/g35434.1.
- 474 Kalnay, E., Kanamitsu, M., Kistler, R., Collins, W., Deaven, D., Gandin, L., Iredell, M., Saha, S., White, G.,  
475 Woollen, J., and et al., 1996, The NCEP/NCAR 40-year reanalysis project: *Bulletin of the American  
476 Meteorological Society*, vol. 77, pp. 437–471, doi:10.1175/1520-0477(1996)077<437:tnyrp>2.0.co;2.
- 477 Kasbohm, J. and Schoene, B., 2018, Rapid eruption of the Columbia River flood basalt and correlation with the  
478 mid-Miocene climate optimum: *Science Advances*, vol. 4, pp. 1–8, doi:10.1126/sciadv.aat8223.
- 479 Kent, D. V. and Muttoni, G., 2008, Equatorial convergence of india and early Cenozoic climate trends: *Proceedings  
480 of the National Academy of Sciences*, vol. 105, pp. 16,065–16,070, doi:10.1073/pnas.0805382105.
- 481 Kent, D. V. and Muttoni, G., 2013, Modulation of Late Cretaceous and Cenozoic climate by variable drawdown of  
482 atmospheric pCO<sub>2</sub> from weathering of basaltic provinces on continents drifting through the equatorial humid  
483 belt: *Climate of the Past*, vol. 9, pp. 525–546, doi:10.5194/cp-9-525-2013.
- 484 Khudoley, A. K., Prokopiev, A. V., Chamberlain, K. R., Ernst, R. E., Jowitt, S. M., Malyshev, S. V., Zaitsev, A. I.,  
485 Kropachev, A. P., and Koroleva, O. V., 2013, Early Paleozoic mafic magmatic events on the eastern margin of  
486 the Siberian craton: *Lithos*, vol. 174, pp. 44–56, doi:10.1016/j.lithos.2012.08.008.

- 487 Kingsbury, C. G., Kamo, S. L., Ernst, R. E., Söderlund, U., and Cousens, B. L., 2018, U-Pb geochronology of the  
488 plumbing system associated with the Late Cretaceous Strand Fiord Formation, Axel Heiberg Island, Canada:  
489 part of the 130–90 Ma High Arctic large igneous province: *Journal of Geodynamics*, vol. 118, pp. 106–117,  
490 doi:10.1016/j.jog.2017.11.001.
- 491 Kirschvink, J. L., 1992, Late Proterozoic low-latitude global glaciation: The Snowball Earth: *In* Schopf, J., Klein,  
492 C., and Des Maris, D., eds., *The Proterozoic Biosphere: A Multidisciplinary Study*, Cambridge University Press,  
493 pp. 51–52.
- 494 Kump, L. R. and Arthur, M. A., 1997, Global Chemical Erosion during the Cenozoic: Weatherability Balances the  
495 Budgets, Springer US, Boston, MA, pp. 399–426: doi:10.1007/978-1-4615-5935-1\_18.
- 496 Larsen, L. M., Pedersen, A. K., Tegner, C., Duncan, R. A., Hald, N., and Larsen, J. G., 2015, Age of Tertiary  
497 volcanic rocks on the West Greenland continental margin: volcanic evolution and event correlation to other parts  
498 of the North Atlantic Igneous Province: *Geological Magazine*, vol. 153, pp. 487–511,  
499 doi:10.1017/s0016756815000515.
- 500 Li, Z. X., Bogdanova, S. V., Collins, A. S., Davidson, A., Waele, B. D., Ernst, R. E., Fitzsimons, I. C. W., Fuck,  
501 R. A., Gladkochub, D. P., Jacobs, J., Karlstrom, K. E., Lu, S., Natapov, L. M., Pease, V., Pisarevsky, S. A.,  
502 Thrane, K., and Vernikovsky, V., 2008, Assembly, configuration, and break-up history of Rodinia: a synthesis:  
503 *Precambrian Research*, vol. 160, pp. 179–210, doi:10.1016/j.precamres.2007.04.021.
- 504 Loewen, M. W., Duncan, R. A., Kent, A. J. R., and Krawl, K., 2013, Prolonged plume volcanism in the Caribbean  
505 large igneous province: New insights from Curaçao and Haiti: *Geochemistry, Geophysics, Geosystems*, vol. 14,  
506 pp. 4241–4259, doi:10.1002/ggge.20273.
- 507 Macdonald, F. A., Schmitz, M. D., Crowley, J. L., Roots, C. F., Jones, D. S., Maloof, A. C., Strauss, J. V., Cohen,  
508 P. A., Johnston, D. T., and Schrag, D. P., 2010, Calibrating the Cryogenian: *Science*, vol. 327, pp. 1241–1243,  
509 doi:10.1126/science.1183325.
- 510 Macdonald, F. A., Swanson-Hysell, N. L., Park, Y., Lisiecki, L., and Jagoutz, O., 2019, Arc-continent collisions in  
511 the tropics set Earth's climate state: *Science*, vol. 364, pp. 181–184, doi:10.1126/science.aav5300.
- 512 Macdonald, F. A. and Wordsworth, R., 2017, Initiation of Snowball Earth with volcanic sulfur aerosol emissions:  
513 *Geophysical Research Letters*, vol. 44, pp. 1938–1946, doi:10.1002/2016GL072335.
- 514 MacLennan, S. A., Park, Y., Swanson-Hysell, N. L., Maloof, A. C., Schoene, B., Gebreslassie, M., Antilla, E.,  
515 Tesema, T., Alene, M., and Haileab, B., 2018, The arc of the Snowball: U-Pb dates constrain the Islay anomaly  
516 and the initiation of the Sturtian glaciation: *Geology*, vol. 46, pp. 539–542, doi:10.1130/G40171.1.
- 517 Maher, K. and Chamberlain, C. P., 2014, Hydrologic regulation of chemical weathering and the geologic carbon  
518 cycle: *Science*, vol. 343, pp. 1502–1504, doi:10.1126/science.1250770.
- 519 Manabe, S., 1969, Climate and the ocean circulation: the atmospheric circulation and the hydrology of the Earth's  
520 surface: *Monthly Weather Review*, vol. 97, pp. 739–774, doi:10.1175/1520-0493(1969)097<739:catoc>2.3.co;2.
- 521 Michel, L. A., Tabor, N. J., and Montañez, I. P., 2016, Paleosol diagenesis and its deep-time paleoenvironmental  
522 implications, Pennsylvanian-Permian Lodève Basin, France: *Journal of Sedimentary Research*, vol. 86, pp.  
523 813–829, doi:10.2110/jsr.2016.41.
- 524 Montañez, I. P., 2013, Modern soil system constraints on reconstructing deep-time atmospheric co<sub>2</sub>: *Geochimica et  
525 Cosmochimica Acta*, vol. 101, pp. 57–75, doi:10.1016/j.gca.2012.10.012.
- 526 Murphy, J. B., van Staal, C. R., and Keppie, J. D., 1999, Middle to late Paleozoic Acadian orogeny in the northern  
527 Appalachians: A Laramide-style plume-modified orogeny?: *Geology*, vol. 27, pp. 653–656,  
528 doi:10.1130/0091-7613(1999)027<653:mtlpa>2.3.co;2.

- 529 Park, Y., Swanson-Hysell, N. L., MacLennan, S. A., Maloof, A. C., Gebreslassie, M., Tremblay, M. M., Schoene, B.,  
530 Alene, M., Anttila, E., Tesema, T., and Haileab, B., in review, The lead-up to the Sturtian Snowball Earth:  
531 Neoproterozoic chemostratigraphy time-calibrated by the Tambien Group of Ethiopia: GSA Bulletin.
- 532 Pirajno, F. and Hoatson, D. M., 2012, A review of Australia's large igneous provinces and associated mineral  
533 systems: Implications for mantle dynamics through geological time: Ore Geology Reviews, vol. 48, pp. 2–54,  
534 doi:10.1016/j.oregeorev.2012.04.007.
- 535 Pujol, M., Marty, B., Burgess, R., Turner, G., and Philippot, P., 2013, Argon isotopic composition of Archaean  
536 atmosphere probes early Earth geodynamics: Nature, vol. 498, pp. 87–90, doi:10.1038/nature12152.
- 537 Ricci, J., Quidelleur, X., Pavlov, V., Orlov, S., Shatsillo, A., and Courtillot, V., 2013, New  $^{40}\text{Ar}/^{39}\text{Ar}$  and K-Ar  
538 ages of the Viluy traps (Eastern Siberia): Further evidence for a relationship with the Frasnian-Famennian mass  
539 extinction: Palaeogeography, Palaeoclimatology, Palaeoecology, vol. 386, pp. 531–540,  
540 doi:10.1016/j.palaeo.2013.06.020.
- 541 Schaller, M. F., Wright, J. D., and Kent, D. V., 2011, Atmospheric pCO<sub>2</sub> perturbations associated with the Central  
542 Atlantic Magmatic Province: Science, vol. 331, pp. 1404–1409, doi:10.1126/science.1199011.
- 543 Schaller, M. F., Wright, J. D., Kent, D. V., and Olsen, P. E., 2012, Rapid emplacement of the Central Atlantic  
544 Magmatic Province as a net sink for CO<sub>2</sub>: Earth and Planetary Science Letters, vol. 323–324, pp. 27–39,  
545 doi:10.1016/j.epsl.2011.12.028.
- 546 Schoene, B., Samperton, K. M., Eddy, M. P., Keller, G., Adatte, T., Bowring, S. A., Khadri, S. F. R., and Gertsch,  
547 B., 2014, U-Pb geochronology of the Deccan Traps and relation to the end-Cretaceous mass extinction: Science,  
548 vol. 347, pp. 182–184, doi:10.1126/science.aaa0118.
- 549 Shevenell, A. E., 2004, Middle Miocene Southern Ocean cooling and Antarctic cryosphere expansion: Science, vol.  
550 305, pp. 1766–1770, doi:10.1126/science.1100061.
- 551 Swanson-Hysell, N. L., Kilian, T. M., and Hanson, R. E., 2015, A new grand mean palaeomagnetic pole for the 1.11  
552 Ga Umkondo large igneous province with implications for palaeogeography and the geomagnetic field:  
553 Geophysical Journal International, vol. 203, pp. 2237–2247, doi:10.1093/gji/ggv402.
- 554 Swanson-Hysell, N. L. and Macdonald, F. A., 2017, Tropical weathering of the Taconic orogeny as a driver for  
555 Ordovician cooling: Geology, vol. 45, pp. 719–722, doi:10.1130/G38985.1.
- 556 Swanson-Hysell, N. L., Ramezani, J., Fairchild, L. M., and Rose, I. R., 2019, Failed rifting and fast drifting:  
557 Midcontinent Rift development, Laurentia's rapid motion and the driver of Grenvillian orogenesis: GSA Bulletin,  
558 doi:10.1130/b31944.1.
- 559 Thorne, J., Cooper, M., and Claoué-Long, J., 2014, Guide to using the Australian mafic-ultramafic magmatic  
560 events GIS dataset: Archean, Proterozoic and Phanerozoic magmatic events: Geoscience Australia,  
561 doi:10.11636/record.2014.039.
- 562 Torsvik, T. H. and Cocks, L. R. M., 2016, Earth History and Palaeogeography: Cambridge University Press,  
563 doi:10.1017/9781316225523.
- 564 Trenberth, K. E., Fasullo, J. T., and Mackaro, J., 2011, Atmospheric moisture transports from ocean to land and  
565 global energy flows in reanalyses: Journal of Climate, vol. 24, pp. 4907–4924, doi:10.1175/2011jcli4171.1.
- 566 Trenberth, K. E., Stepaniak, D. P., and Caron, J. M., 2000, The global monsoon as seen through the divergent  
567 atmospheric circulation: Journal of Climate, vol. 13, pp. 3969–3993,  
568 doi:10.1175/1520-0442(2000)013<3969:tgmast>2.0.co;2.
- 569 West, A. J., 2012, Thickness of the chemical weathering zone and implications for erosional and climatic drivers of  
570 weathering and for carbon-cycle feedbacks: Geology, vol. 40, pp. 811–814, doi:10.1130/g33041.1.

- 571 Xu, Y.-G., Wei, X., Luo, Z.-Y., Liu, H.-Q., and Cao, J., 2014, The Early Permian Tarim large igneous province:  
572 Main characteristics and a plume incubation model: *Lithos*, vol. 204, pp. 20–35, doi:10.1016/j.lithos.2014.02.015.
- 573 Zhai, Q.-g., Jahn, B.-m., Su, L., Ernst, R. E., Wang, K.-l., Zhang, R.-y., Wang, J., and Tang, S., 2013, SHRIMP  
574 zircon U-Pb geochronology, geochemistry and Sr-Nd-Hf isotopic compositions of a mafic dyke swarm in the  
575 Qiangtang terrane, northern Tibet and geodynamic implications: *Lithos*, vol. 174, pp. 28–43,  
576 doi:10.1016/j.lithos.2012.10.018.
- 577 Zhou, M.-F., Malpas, J., Song, X.-Y., Robinson, P. T., Sun, M., Kennedy, A. K., Lesher, C., and Keays, R. R.,  
578 2002, A temporal link between the Emeishan large igneous province (SW China) and the end-Guadalupian mass  
579 extinction: *Earth and Planetary Science Letters*, vol. 196, pp. 113–122, doi:10.1016/s0012-821x(01)00608-2.
- 580 Zhu, D.-C., Chung, S.-L., Mo, X.-X., Zhao, Z.-D., Niu, Y., Song, B., and Yang, Y.-H., 2009, The 132 Ma  
581 Comei-Bunbury large igneous province: Remnants identified in present-day southeastern Tibet and southwestern  
582 Australia: *Geology*, vol. 37, pp. 583–586, doi:10.1130/g30001a.1.